JOURNAL OF GEOPHYSICAL RESEARCH, VOL. 101, NO. A4, PAGES 7659–7676, APRIL 1, 1996

A study of Uranus' bow shock motions using Langmuir waves

S. Xue [1] and I. H. Cairns
Department of Physics and Astronomy, University of Iowa, Iowa City

C. W. Smith
Bartol Research Institute, University of Delaware, Newark

D. A. Gurnett
Department of Physics and Astronomy, University of Iowa, Iowa City

Abstract. During the Voyager 2 flyby of Uranus, strong electron plasma oscillations (Langmuir waves) were detected by the plasma wave instrument in the 1.78-kHz channel on January 23-24, 1986, prior to the inbound bow shock crossing. Langmuir waves are excited by energetic electrons streaming away from the bow shock. The goal of this work is to estimate the location and motion of Uranus' bow shock using Langmuir wave data, together with the spacecraft positions and the measured interplanetary magnetic field. The following three remote sensing analyses were performed: the basic remote sensing method, the lag time method, and the trace-back method. Because the interplanetary magnetic field was highly variable, the first analysis encountered difficulties in obtaining a realistic estimation of Uranus' bow shock motion. In the lag time method developed here, time lags due to the solar wind's finite convection speed are taken into account when calculating the shock's standoff distance. In the new trace-back method, limits on the standoff distance are obtained as a function of time by reconstructing electron paths. Most of the results produced by the latter two analyses are consistent with predictions based on the standard theoretical model and the measured solar wind plasma parameters. Differences between our calculations and the theoretical model are discussed.

1. Introduction

It is known that electron plasma oscillations, which are generally called Langmuir waves, occur upstream from planetary bow shocks [*Scarf et al.*, 1971, 1979; *Anderson et al.*, 1981; *Gurnett et al.*, 1981, 1986, 1989]. When observed, these waves provide evidence that the spacecraft is magnetically connected to and often close to the bow shock. During the Voyager 2 spacecraft's flyby of Uranus on January 23-24, 1986, high levels of Langmuir waves were detected by the plasma wave instrument near 1.78 kHz prior to the inbound bow shock crossing. The Langmuir waves occurred in sporadic bursts for about 1 day until the spacecraft finally crossed the bow shock around 0730 spacecraft event time (SCET) on January 24, 1986. (Hereafter all times are displayed in the hour-minute format and the SCET label is suppressed.)

[1]Now at Department of Space Physics and Astronomy, Rice University, Houston, Texas.

Paper number 95JA03849.
0148-0227/96/95JA-03849$05.00

The region upstream from a bow shock is divided into the following three subregions: the undisturbed solar wind, the electron foreshock which is dominated by electrons escaping from the shock, and the ion foreshock which is dominated by ions escaping from the shock. Figure 1 shows the expected relationships between Uranus' bow shock, the electron and ion foreshocks, and the tangent magnetic field line. The expected time history of the Langmuir electric field amplitude E_L along the spacecraft trajectory is also shown. Charged particles propagate along the interplanetary magnetic field (IMF) lines, undergo a downstream directed $\mathbf{E} \times \mathbf{B}$ drift due to the solar wind's convection electric field, and undergo the usual cyclotron motion. The $\mathbf{E} \times \mathbf{B}$ drift then requires the upstream boundary of the electron foreshock to be slightly downstream from the locus of B-field lines tangent to the bow shock. The ion foreshock boundary is located downstream from the electron foreshock boundary because of the ions' relatively low speeds. Langmuir waves are excited by electrons with high speeds, $\gtrsim 10^7\,\mathrm{m\,s^{-1}}$, streaming into the solar wind upstream from the bow shock. The commonly accepted generation mechanism for these Langmuir waves [*Scarf et al.*, 1971; *Filbert and Kellogg*, 1979;

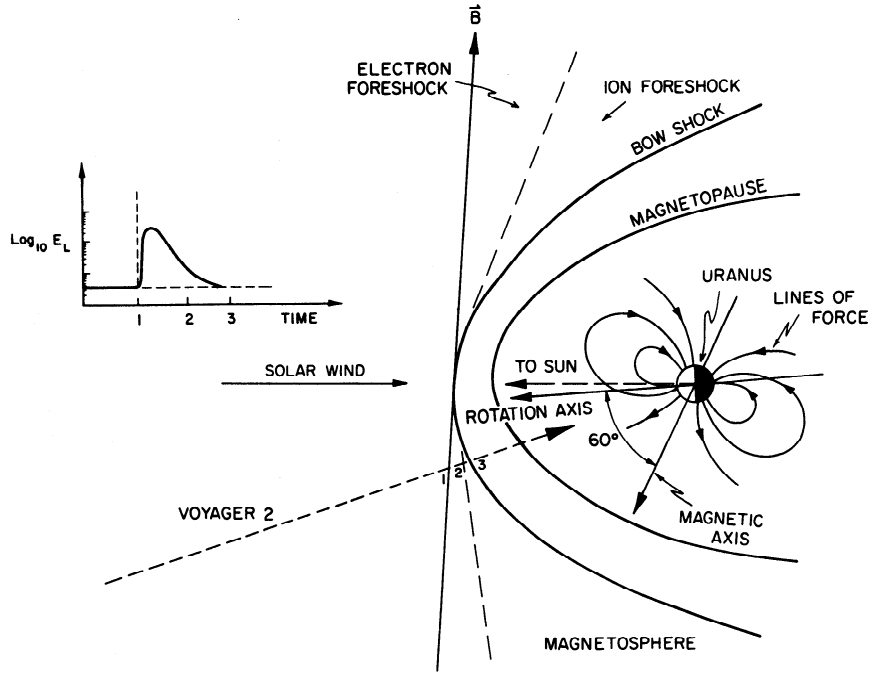

Figure 1. A schematic picture showing the tangent magnetic field line, the electron and ion foreshocks, and the bow shock of Uranus. The magnetopause and the planet's dipole magnetic field are also drawn. The time history of the Langmuir electrical field strength E_L along the spacecraft trajectory is also shown (top left).

Cairns, 1987a, b] is the classical two-stream instability, otherwise known as the bump-on-tail instability.

High levels of Langmuir waves should be detected near and slightly downstream from the electron foreshock boundary. At Earth the field amplitudes decrease substantially downstream from the foreshock boundary, and only very low levels are observed in the ion foreshock [e.g., *Filbert and Kellogg*, 1979; *Anderson et al.*, 1981; *Etcheto and Faucheux*, 1984; *Fuselier et al.*, 1985; *Klimas*, 1985]. If relatively high levels of Langmuir waves are observed, then the tangent magnetic field line must be very close to the position of the spacecraft. Different, well-separated Langmuir wave bursts correspond to different electron foreshock crossings. (Burstiness on timescales ~1 s is also observed at constant positions in a foreshock, analagous to the clumping of Langmuir waves in type III sources; stochastic growth theory [e.g., *Robinson et al.*, 1993] likely explains these short-timescale foreshock bursts.) The crossings may be due to movement of the bow shock or the spacecraft or to changes in the IMF orientation. The location and/or shape of a bow shock can therefore be inferred remotely using the spacecraft positions and measured IMF vectors when Langmuir waves start and/or stop [*Cairns et al.*, 1991] (cf. *Fuselier et al.*'s [1986] analysis for electron events.).

Variations in the solar wind's ram pressure P_{sw}, the sonic, Alfvén, and fast magnetosonic Mach numbers, and the IMF orientation change the location and shape of planetary bow shocks [e.g., *Spreiter et al.*, 1966; *Fairfield*, 1971; *Formisano et al.*, 1971; *Slavin and Holzer*, 1981; *Slavin et al.*, 1985; *Farris et al.*, 1991; *Cairns and Grabbe*, 1994; *Cairns et al.*, 1995; *Cairns and Lyon*, 1995]. On the other hand, as suggested by *Ness et al.* [1986] for Uranus and by *Belcher et al.* [1989], *Ness et al.* [1989], and *Voigt and Ness* [1990] for Neptune, the rotation of a planet's oblique, tilted magnetic field should cause periodic changes in the location and/or shape of the magnetopause. Variations in the location and/or shape of the planet's bow shock may accompany these magnetopause changes. Evidence for rotational control of the location of Neptune's bow shock exists [*Cairns et al.*, 1991; *Szabo*, 1992]. *Ness et al.* [1986] have explicitly suggested such changes for the Uranus bow shock. We have therefore performed three types of remote-sensing analyses in order to estimate the location and motion of Uranus' bow shock as a function of time. These analyses are the basic remote sensing analysis [*Cairns et al.*, 1991] and two modified analyses developed here, the lag time method and the trace-back method.

This paper is organized as follows. Section 2 describes the Langmuir wave and IMF observations. Section 3 describes the basic remote sensing analysis. However, because the observed IMF fluctuated rapidly, this analysis results in standoff distances that are unreasonable when compared with those predicted by pressure balance considerations. Difficulties in this method are discussed. In sections 4 and 5, two modified remote sensing techniques, the lag time method and the trace-back method, are developed and applied. The lag time method takes into account the time required for con-

vection of favorable magnetic field orientations to the shock. The trace-back method involves reconstructing electron paths as a function of time. Section 6 compares our results with predictions from the standard theoretical model for planetary bow shocks; quite good agreement is found between the remotely sensed and the predicted shock locations. The conclusions are presented in section 7.

2. Description of Measurements

Plasma Wave Data

In January 1986, Voyager 2 flew through the Uranian system. The electric field amplitudes of various plasma waves were measured by the 16-channel spectrum analyzer of the Voyager plasma wave (PWS) instrument [*Scarf and Gurnett*, 1977]. A complete plasma wave spectrum is collected from 10 Hz to 56.2 kHz every 4 s.

Langmuir waves, otherwise known as electron plasma oscillations, can be easily identified in the plasma wave data because they usually occur in only one channel or two neighboring channels near the local electron plasma oscillation frequency f_p. The plasma frequency depends on the square root of the local electron density: $f_p = 9000\sqrt{n_e}$ Hz, where n_e is in units of cm^{-3}. *Bridge et al.* [1986] reported that typically, $n_e \sim 0.025$ cm^{-3} in the solar wind upstream from Uranus' bow shock. This implies that $f_p \approx 1.4$ kHz. The first clear evidence of Langmuir waves associated with the bow shock occurred at 0550 on January 23, 1986, when a strong burst of electron plasma oscillations was recorded in the 1.78-kHz PWS channel. The plasma oscillations then continued sporadically for about 1 day until the spacecraft eventually crossed the bow shock at 0728 on January 24 [*Gurnett et al.*, 1986]. Figure 2 shows the Langmuir wave bursts appearing in the 1.78-kHz channel and its neighboring channels from 0500 on day 23 to 0900 on day 24.

Magnetic Field Data

Behannon et al. [1977] described the magnetic field instrument on the Voyager 2 spacecraft. R. P. Lepping (personal communication, 1991) provided 1.92-s averages of the 60-ms vector IMF measurements from the Voyager magnetometer in the usual solar equatorial radial, tangential, normal (RTN) coordinate system. These vectors were converted from the RTN system to a Uranus-centered x-y-z coordinate system (defined in section 3) using rotation matrices provided by N. Bachman (personal communication, 1992). An approximate relation between the two coordinate systems is $(B_x, B_y, B_z) \approx (-B_r, -B_t, B_n)$. The average IMF strength prior to the Uranus encounter is very low ($\sim$0.1 nT). However, spacecraft roll maneuvers during the planetary encounter permitted experimenters to establish absolute uncertainties of 0.006 nT for each individual field component [*Lepping et al.*, 1989; R. P. Lepping, personal communications, 1992], a factor of $\sim$15 less than the typical IMF level. The magnetic field data are therefore suitable for remote sensing analyses.

3. Basic Remote Sensing Analysis

As previously described, energetic electrons streaming away from the bow shock and the resulting Langmuir waves are constrained to lie in the electron foreshock. The highest levels of Langmuir waves appear

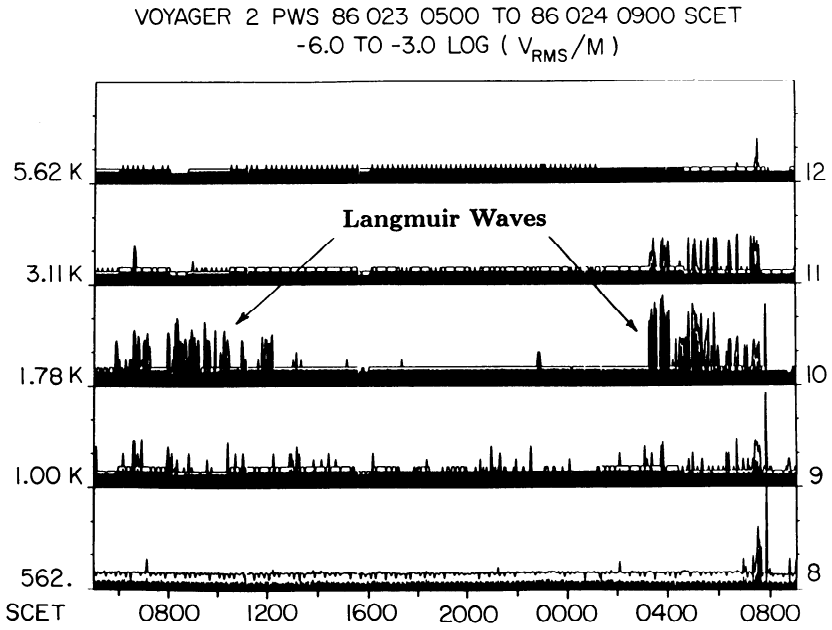

Figure 2. Langmuir waves recorded in the 1.78-kHz channel and the neighboring channels (3.11 kHz or 1.00 kHz) before the inbound bow shock crossing of Voyager 2.

very close to the electron foreshock boundary [e.g., *Filbert and Kellogg*, 1979; *Etcheto and Faucheux*, 1984; *Klimas*, 1985]. Changes in IMF direction or the shock's location, as well as the spacecraft's motion, can result in the spacecraft entering or exiting the electron foreshock, thereby resulting in the appearance or disappearance of Langmuir waves. Since the $\mathbf{E}\times\mathbf{B}$ drift speed V_d is much less than the electron's speed $V_\parallel$ parallel to $\mathbf{B}$, $V_d \ll V_\parallel$, electron beams can be assumed to move along magnetic field lines. When an intense Langmuir burst is observed, the measured (and appropriately averaged) IMF vector should connect the spacecraft to the near vicinity of the tangent point on the shock [*Cairns et al.*, 1991]. A Uranus-centered system is used; the x axis points sunward from Uranus, the y axis lies antiparallel to Uranus' orbital velocity in the orbital plane, and the z axis completes a right-handed coordinate system. The bow shock is assumed to have a paraboloidal shape that is symmetric about the Sun-Uranus line:

$$x = a_s - b_s(y^2 + z^2). \tag{1}$$

Here the parameter a_s is the standoff distance (or nose position) and the parameter b_s refers to the shape of the shock. While bow shocks are probably best modeled as hyperboloids, ellipsoid and paraboloid fits are common. However, ellipsoid fits are inaccurate once near or downstream from the terminator. In contrast, a hyperboloid can be fit very accurately by a paraboloid, except very far down the flanks of the shock. A paraboloidal shock model is used here for the following three additional reasons: algebraic simplicity, computational ease, and convention in connection analyses [e.g., *Filbert and Kellogg*, 1979; *Fuselier et al.*, 1986; *Cairns et al.*, 1991]. Aberration of the bow shock due to Uranus' orbital motion around the Sun is of order 0.9° and is neglected here.

Using the Voyager 2 inbound and outbound bow shock crossings [*Bridge et al.*, 1986; *Gurnett et al.*, 1986; *Ness et al.*, 1986] and (1), a nominal shock model is calculated as follows: $a_s = 23.4\,R_U$ and $b_s = 0.02\,R_U^{-1}$, where R_U (25,600 km) is Uranus' radius. Uranus' bow shock is a high Mach number (fast magnetosonic number $\overline{M}_{\rm MS} > 15$) shock [*Bagenal et al.*, 1987]. Accordingly, changes in the shock shape (related to b_s) caused by changes in Mach number are negligible. Variations in the solar wind ram pressure P_{sw} also affect the location and shape of the magnetopause and therefore the shock [e.g., *Binsack and Vasyliunas*, 1968; *Fairfield*, 1971; *Slavin et al.*, 1985]. According to observations [e.g., *Binsack and Vasylinuas*, 1968] and MHD theory, the Earth's bow shock varies self-similarly with P_{sw} variations, so that $a_s \propto P_{sw}^{-1/6}$. That is, the bow shock undergoes an expansion or contraction in response to a change in P_{sw}. Considering our shock model, self-similarity with $a_s \propto P_{sw}^{-1/6}$ requires $b_s \propto P_{sw}^{+1/6}$. Therefore in the analyses below for a_s we assume that the shock's shape parameter b_s satisfies

$$b_s = b_{s0}(P_{sw}/P_0)^{1/6}, \tag{2}$$

where $b_{s0} = 0.02\,R_U^{-1}$ and $P_0 = 1.69\times10^{-2}$ nPa are the nominal values corresponding to the observed inbound shock crossing.

As the spacecraft enters or exits the electron foreshock, Langmuir waves appear or disappear, so that one can thereby identify the foreshock boundary (tangent magnetic field line). Constraints on a_s and b_s follow on combining the locations of foreshock crossings with magnetic field data. The magnetic field line with orientation (B_x, B_y, B_z) that passes through the spacecraft position (x_{sc}, y_{sc}, z_{sc}) is assumed to be straight with

$$\frac{x - x_{sc}}{B_x} = \frac{y - y_{sc}}{B_y} = \frac{z - z_{sc}}{B_z} = t, \tag{3}$$

where the point (x, y, z) lies on this straight line. When Langmuir waves appear, this straight magnetic field line should be a tangent to the bow shock (by assumption). Therefore by solving (1) and (3) simultaneously, a constraint on a_s and b_s is constructed using the spacecraft position and the magnetic field components [e.g., *Fuselier et al.*, 1986; *Cairns et al.*, 1991]:

$$a_s = x_{sc} - \frac{B_x^2}{4b_s\alpha} - \frac{\beta B_x}{\alpha} - \frac{\beta^2 b_s}{\alpha} + \gamma b_s \tag{4}$$

where $\alpha = B_y^2 + B_z^2, \beta = y_{sc}B_y + z_{sc}B_z$, and $\gamma = y_{sc}^2 + z_{sc}^2$.

Each foreshock crossing specifies a version of (4) that relates a_s and b_s. Obviously, we need to identify two foreshock crossings with different magnetic field orientations and spacecraft positions to calculate a_s and b_s independently [e.g., *Cairns et al.*, 1991]. This procedure has the disadvantage that the bow shock is assumed implicitly to be at the same location for the two foreshock boundary crossings, which may or may not be correct. An alternative procedure is to first calculate the shock's shape (i.e., b_s) by assuming that it varies as $P_{sw}^{+1/6}$, as justified earlier. Then, (3) can be used to infer a_s for each foreshock crossing, thereby allowing study of changes in a_s with time.

These procedures for determining the location and/or shape of the bow shock involve several implicit assumptions. First, the analysis assumes that large-scale changes in the IMF orientation or the shock's position cause the foreshock to sweep back and forth across the spacecraft. Second, the magnetic field is assumed to stretch in straight lines from the spacecraft to the tangent point. These two assumptions require that representative large-scale magnetic field vectors be used in the analysis. Both time averaging (to reduce local fluctuations) and distance averaging (to achieve a truly large-scale field) of the measured field should therefore be performed. Third, electron beams need finite times to travel from the shock to the spacecraft. Assuming beam speeds of order $\sim10^7$–10^8 m s^{-1} electrons travel $\sim$20–200 R_U min^{-1}, respectively. Accordingly, for typical spacecraft-tangent point distances $\gtrsim 20\,R_U$, relatively stable or long-lived (about 1 min or longer) Langmuir wave events should be analyzed.

The following "basic" remote sensing analysis can be performed [*Cairns et al.*, 1991]: construct averaged IMF vectors for each foreshock crossing by averaging over the event interval (thereby reducing the effects of local fluctuations in the field direction) and estimate a_s for each event using (4). We followed this procedure for the events on January 23 and 24 using two choices for b_{s0}, $0.02\,R_U^{-1}$ and $0.018\,R_U^{-1}$. Ram pressure-induced variations in b_s are ignored here, as justified in section 6 below. Unfortunately, the resulting a_s values are very large, vary rapidly, and are sometimes negative. For instance, on day 23, a_s is typically $\sim 40-80\,R_U$ but varied by $\sim 90\ R_U$ in ~ 4 hours, while on day 24, a_s ranged from ~ 0 to $20\ R_U$ from about 0315–0340. Remembering that a_s is nominally of order $23\,R_U$, that Mach number effects should be insignificant at Uranus, and that $a_s \propto P_{sw}^{-1/6}$ nominally, these inferred variations in a_s would correspond to P_{sw} changing by factors $\sim 4^6 = 4096$ on days 23 and 24, inconsistent with in situ Voyager plasma data. However, on day 24, from about 0350 until the inbound shock crossing, the computed a_s values varied between 23 and $31\,R_U$. As shown below, these a_s values are consistent with our other analyses.

The above results imply that the basic remote sensing analysis is inapplicable to the data on day 23 and only partially applicable on day 24. This limitation can be understood in terms of difficulties in constructing representative large-scale magnetic fields. First, note that the electrons driving the waves move much faster than the solar wind speed. Since the IMF is "frozen in" to the solar wind, the energetic electrons actually travel primarily along different magnetic fields lines from the locally measured ones. Second, the observed magnetic field vectors fluctuate significantly over 1 min timescales (see Figure 4 below). This sometimes makes the electron trajectories very complicated, thereby causing problems in constructing a representative large-scale field. This problem is particularly serious on day 23, when the spacecraft was very far from the bow shock ($\sim 65-80\,R_U$). Third, the assumption of straight field lines is not always justified, primarily due to significant temporal/spatial variations in the observed magnetic field. Fortunately, these difficulties have been ameliorated by developing and using two new methods, the lag time and trace-back methods, described below.

In summary, the basic remote sensing analysis used by *Cairns et al.* [1991] at Neptune encounters difficulties at Uranus due to the IMF typically varying substantially between the spacecraft and the bow shock. These difficulties were minimal at Neptune because the IMF was relatively stable and the convection distance relatively small.

4. The Lag Time Method

In the previous analysis, solar wind convection was neglected due to the solar wind speed ($\sim 470\,\mathrm{km\,s^{-1}}$) being very small compared to the electron streaming speed ($\sim 10^7-10^8\,\mathrm{m\,s^{-1}}$). However, the unexpectedly large IMF fluctuations and more distant Langmuir wave detections at Uranus result in the solar wind convection being very important. This is due to a time lag existing between the time when magnetic field lines favorable for connection of the spacecraft to the bow shock reach the spacecraft and the time when they reach the shock. This time lag can be used to calculate a_s as a function of time and the modified analysis is called the lag time method below. Several relevant concepts and the method itself will be presented in this section.

Definition of DIFF

Filbert and Kellogg [1979] introduced the quantity DIFF to describe the distance of the spacecraft downstream from the electron foreshock boundary, i.e., the displacement of the spacecraft from the tangent field line along the Sun-Uranus line (Figure 3). DIFF is defined in the plane containing both $\mathbf{B}$ and $\mathbf{V}_{sw}$. Electron trajectories lie in this plane [*Cairns*, 1987a], and the parabola is the intersection of the plane with the bow shock. If DIFF > 0, the spacecraft is downstream from the electron foreshock boundary, i.e., in the region with streaming charged particles. When DIFF < 0, the spacecraft is located upstream from the foreshock and so, according to standard theory [*Filbert and Kellogg*, 1979; *Cairns*, 1987a, b], no Langmuir waves should be observed. Langmuir waves with large amplitudes should be detected when DIFF is positive but relatively small (in the forward edge of the foreshock). As DIFF increases from zero, the wave level decreases dramatically, so that the waves should be extremely weak when deep in the foreshock.

Since DIFF depends on the IMF orientation, the spacecraft position, and the location and shape of the bow shock, the nominal shock model ($a_s = 23.4 R_U, b_s = 0.02\,R_U^{-1}$) has been combined with the IMF and spacecraft trajectory data to compute DIFF for days 23 and 24. Because a nominal shock model is used, qualitative changes in DIFF are of primary importance. Figures 4 and 5 show DIFF computed both with and without averaging the IMF for days 23 and 24, respectively. It can be seen that the unaveraged DIFF values (Figures 4b and 5b) often fluctuate substantially in a very short time period. This is because the local IMF is often highly irregular, especially during the first half of day 23. In order to reduce local "random" variations, we averaged the magnetic field data for 2.5- and 5.0-min periods on days 24 and 23 (Figures 4c and 5c), respectively. Below, we primarily address the DIFF values calculated using the averaged field.

Discussion of DIFF and Langmuir Wave Events

The third panel in Figure 4c shows that DIFF was often very large ($\gtrsim 50\,\mathrm{R_U}$) during the first part of day 23, consistent with the fairly radial IMF direction, implying that the spacecraft was deep in the ion foreshock. However, DIFF often varied rapidly between positive and negative values. The existence of Langmuir wave events is therefore consistent with the standard model

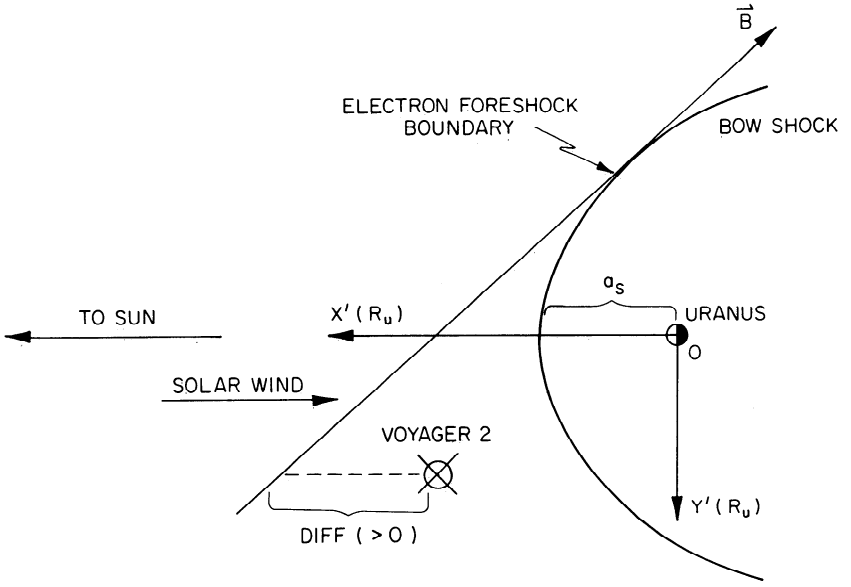

Figure 3. Definition of DIFF. DIFF > 0 when the spacecraft is downstream from the electron foreshock boundary; DIFF < 0 when upstream from the boundary. DIFF is calculated in the plane containing both **B** and $\mathbf{V}_{sw}$; all electron gyrocenter trajectories lie in this plane.

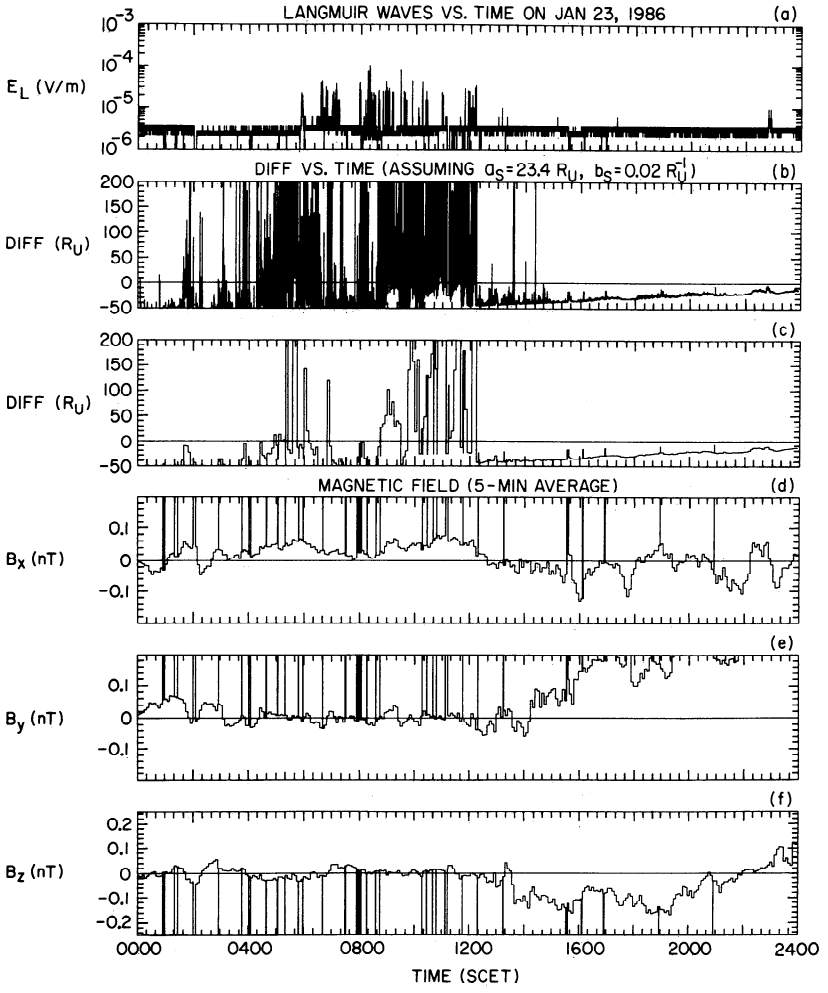

Figure 4. DIFF as a function of time on day 23. (a) Langmuir wave data; DIFF calculated using the (b) unaveraged interplanetary magnetic field (IMF) and (c) 5-min averaged IMF data; and the (d) B_x, (e) B_y, and (f) B_z components of the averaged IMF.

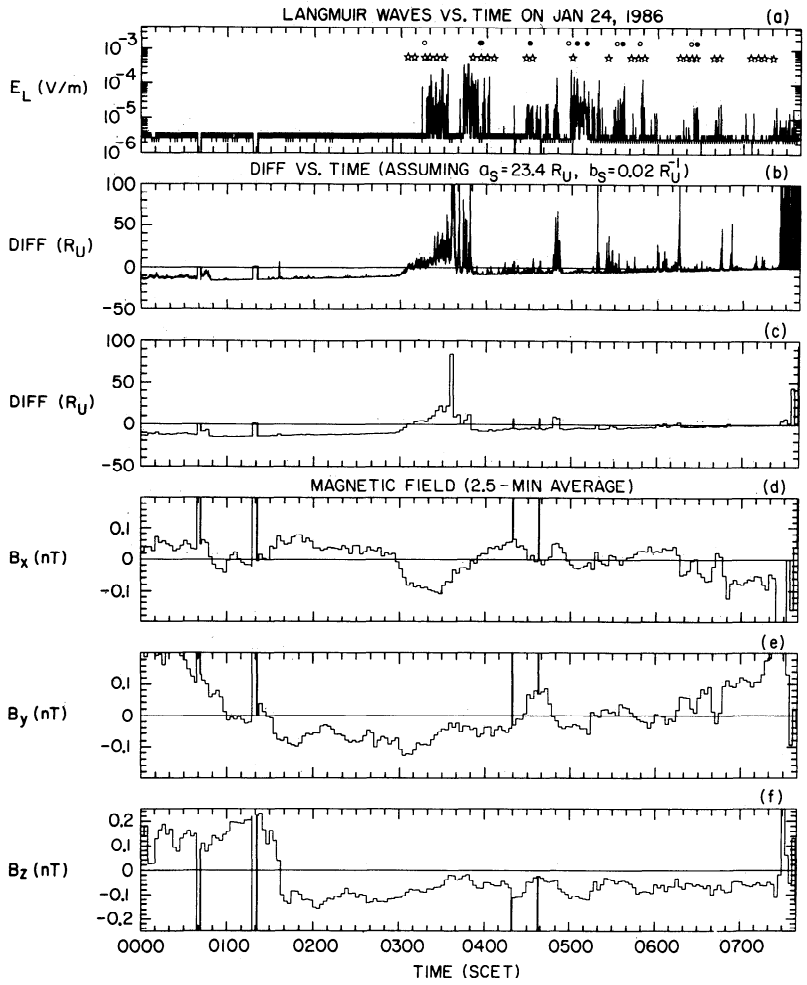

Figure 5. Same as Figure 4, except for on day 24. The wave events or times chosen for the lag time (open circles), lagged-basic (solid circles), and the trace-back analyses (stars) are also shown in Figure 5a.

(DIFF $\sim$ 0). In the second part of day 23 the negative values for DIFF indicate that Voyager is well upstream from the foreshock, consistent with the absence of Langmuir waves.

The DIFF variations on day 24 in Figure 5 are suitable for discussion. DIFF was $\sim -10\,R_U$ before about 0303 (excluding the two short periods centered near $\sim$0045 and $\sim$0120 with missing magnetic field data), when it jumped qualitatively to near zero from negative values. This implies that the spacecraft was initially upstream from the electron foreshock, consistent with the absence of Langmuir waves. From $\sim$0303 to $\sim$0317, there were still no Langmuir waves, although DIFF was now $\sim$0. This period corresponds to a time lag or delay in the appearance of the Langmuir waves and will be discussed in detail later in this section. Starting at $\sim$0320 and ending at $\sim$0332, strong Langmuir waves lasted for $\sim$12 min, while the averaged DIFF values changed from $\sim$5 to $\sim 20\,R_U$. These DIFF values are too large for Voyager to remain in the forward edge of the foreshock unless time-lagged fields, field fluctuations, and finite foreshock size are considered. From 0332 to 0342, DIFF was considerably larger, up to $\sim 50\,R_U$, and no Langmuir waves occurred. This is consistent with Voyager being very deep in the ion foreshock. During the period from $\sim$0343 to $\sim$0354, DIFF switched back qualitatively to around zero (between -9 and $7\,R_U$), consistent with the reappearance of intense Langmuir waves. No waves were observed in the later period 0402–0425, implying that the spacecraft was in the undisturbed solar wind, consistent with DIFF being negative.

During the intervals 0425–0445 and $\sim$0500–0535, DIFF remained small, negative ($-5\,R_U <$ DIFF $< 0\,R_U$), and relatively stable. Meanwhile, Langmuir waves appeared during much of this time. The presence of Langmuir waves implies that the spacecraft was close to the electron foreshock's edge. These events can be understood in terms of the bow shock moving sunward from Uranus; that is, the standoff distances were larger than $23.4\,R_U$ by about $5\,R_U$. Finally, during the period 0600–0613 there were qualitative increases in DIFF but no Langmuir waves. This situation may be interpreted in terms of the spacecraft being deep in the electron

foreshock (probably in the ion foreshock) due to the bow shock moving somewhat sunward. (Alternatively, the shock could be sufficently close to the planet that Voyager remains in the solar wind, but this seems less plausible.) In summary, if time lag effects and shock motions are considered, the observed waves are consistent with standard foreshock theory.

Comparison of DIFF With Previous Work

Krimigis et al. [1988] reported energetic ion enhancements upstream of Uranus' bow shock in the first half of day 23, consistent with our conclusion that Voyager was in the ion foreshock. The absence of ion events for the remainder of day 23 is also consistent with the spacecraft being well upstream from the foreshock (i.e., DIFF $\ll 0$). *Smith et al.* [1989] reported magnetic wave activity during a long interval (~1351–2054) of this day. They suggested that the waves occurred when the inferred large-scale IMF did not connect the spacecraft to the bow shock. This is clearly consistent with the negative values of DIFF calculated for this period, thereby confirming Smith et al.'s suggestion.

One of the discrete ion enhancements on day 24 reported by *Krimigis et al.* peaks near 0340. This ion event occurs in the period 0332–0342 during which DIFF is large and positive and no Langmuir waves occur, thereby providing additional strong evidence that the spacecraft was in the ion foreshock during this interval. Ion events were also found during the intervals 0425–0445 and 0500–0520. As discussed in the previous subsection, Langmuir waves were present during most of these periods and DIFF was small, negative, and relatively stable. This gives rise to the question of how these Langmuir waves can be associated with the observations of ion events. Using the typical energetic ion energy and IMF magnitude observed at Uranus, ~50 keV and ~0.2 nT, respectively, the ion gyroradius is found to be $\sim 5\,R_U$. Accordingly, even if the spacecraft was in the forward edge of electron foreshock rather than in the ion foreshock, the relatively large gyroradius of those ions should make it possible to observe some ions whose gyrocenters are still inside the ion foreshock. The ion observations during the period 0550–0620 evidently support our argument that the spacecraft was in the ion foreshock for the interval 0600–0617.

Both *Russell et al.* [1990] and *Zhang et al.* [1991] searched for low-frequency magnetic waves during the inbound trajectory and found none. The present study reveals two likely reasons for this apparent absence of low-frequency waves. First, the time required to convect the solar wind 50 R_U downstream from the foreshock boundary to the spacecraft is equivalent to only 4.2 proton cyclotron periods. Linear instability theory [e.g., *Gary et al.*, 1984] shows that growth rates for low-frequency upstream waves, assuming typical upstream ion distribution parameters, are comparable to or less than one tenth the ion cyclotron frequency. Observations at Earth [*Bonifazi and Moreno*, 1981] indicate that convection times from the upstream boundary to the spacecraft during wave events exceed at least one growth time. Therefore it is doubtful that DIFF ~50 R_U is sufficient to allow for the excitation of observable upstream waves. Second, the relatively brief penetration of the ion foreshock represents less than one oscillation in the spacecraft frame of reference for upstream waves excited by the resonant instability, the dominant mechanism for upstream wave excitation. Therefore it would be difficult to resolve such a wave, if present.

Time Lag and Favorable Magnetic Fields

Following the discussion of DIFF, we now describe the most important concept in this section: time lag. In ideal MHD theory, magnetic field lines are frozen in the plasma. Regarding the IMF as being fixed in and convected with the solar wind flow permits us to develop a simple model linking changes in DIFF (corresponding to IMF changes) to the appearance and disappearance of Langmuir waves, thereby defining a time lag. Plate 1 illustrates this time lag model schematically, showing the IMF, the Langmuir waves, and DIFF as a function of time. The three subplots at the bottom of Plate show the foreshock geometry and whether or not the spacecraft is magnetically connected to the shock as a function of time. Prior to a certain time T_{Diff}, DIFF is negative, which means the magnetic field lines present at the spacecraft are unfavorable (blue color) for magnetic connection to the bow shock. The spacecraft is upstream from the electron foreshock, and so no Langmuir waves are seen. At time T_{Diff}, DIFF changes qualitatively to a positive value because of a change in the IMF orientation. This implies that favorable magnetic field lines (red color) have been encountered, which, if extrapolated, would connect the spacecraft to the bow shock (see the left subplot in Plate 1, bottom). However, no Langmuir waves are present since the spacecraft is still not magnetically connected to the bow shock. As the favorable field lines convect closer to the planet with the solar wind (see the middle subplot of Plate 1), DIFF remains at the same value. At the later time, T_{Langmuir}, the favorable magnetic field lines eventually reach the bow shock (the right subplot of Plate 1), and subsequently, Langmuir waves occur at the spacecraft. The difference between T_{Diff} and T_{Langmuir} is the time lag T_{Lag}:

$$T_{\mathrm{Lag}} = T_{\mathrm{Langmuir}} - T_{\mathrm{Diff}}. \tag{5}$$

Two possible changes in DIFF may be associated with the Langmuir waves ending. DIFF may increase due to the spacecraft moving deeper into the foreshock (i.e., the dashed line in the plot of DIFF versus time in Plate 1). Otherwise, DIFF becomes negative again due to the spacecraft returning to the solar wind (i.e., the solid line in Plate 1).

The time lag T_{Lag} associates a qualitative change in DIFF with a correlated Langmuir wave event. It indi-

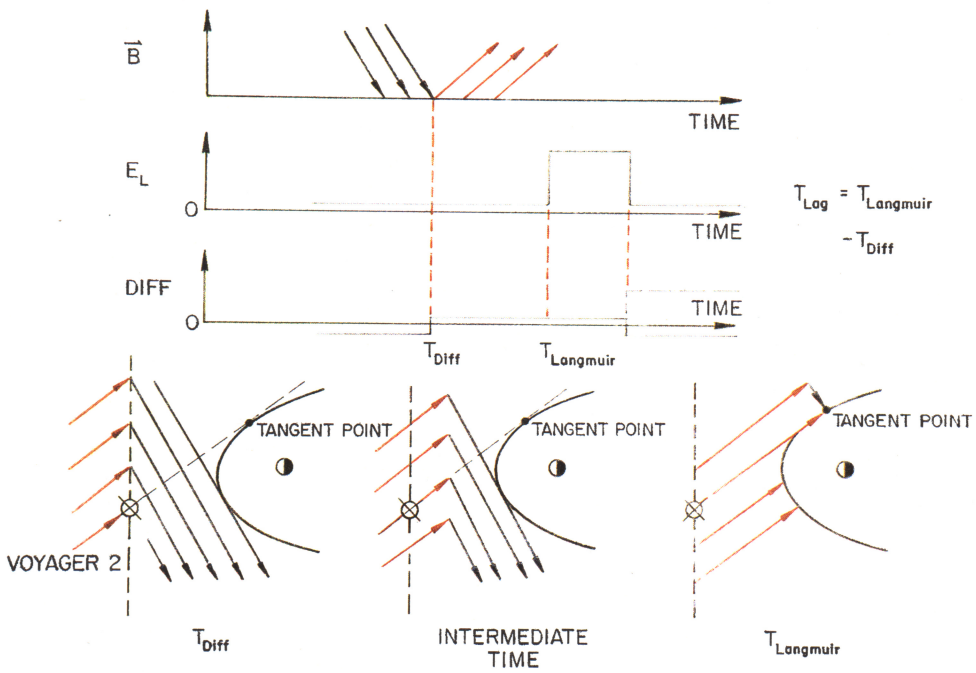

Plate 1. A schematic sketch showing the lag time model. The blue and red arrows indicate the unfavorable and favorable magnetic field lines that the spacecraft meets, respectively. More detailed explanations are given in the text.

cates that the relatively slow solar wind convection of changes in the IMF orientation results in a definite time delay between when favorable field orientations occur at the spacecraft and when the Langmuir waves start. The reason why the basic remote sensing method is often not applicable during times of highly irregular IMF is that time lags are not taken into account.

Theoretical Calculation and Application

Let $\mathbf{x}_T$ denote the position vector of the tangent point T in the Uranus-centered system (x_T, y_T, z_T), while $\mathbf{x}_{sc} = (x_{sc}, y_{sc}, z_{sc})$ is the spacecraft's position vector. The solar wind speed V_{sw} was essentially constant at $\sim$470 km s^{-1} or 1.0 R_U min^{-1} at Uranus, while Voyager 2 traveled at the speed of $\sim 2\,R_U$/h relative to the planet. Thus the spacecraft's speed is negligible relative to V_{sw}. Ignoring the spacecraft motion during the time $T_{\rm Lag}$, the following relation is clear:

$$x_{sc} - x_T = T_{\rm Lag}\, V_{sw}. \tag{6}$$

Note again that the electrons move in planes parallel to the plane containing **B** and the x axis ($\mathbf{V}_{sw}$) [*Cairns*, 1987a]. The original coordinate axes xyz are therefore rotated about the x axis to a new coordinate system (x', y', z') in which $B_{z'} = 0$. If the rotation angle is α, then the new coordinates are related to the old coordinates by

$$\begin{aligned} x' &= x \\ y' &= y\cos\alpha + z\sin\alpha \\ z' &= -y\sin\alpha + z\cos\alpha, \end{aligned} \tag{7}$$

where $\sin\alpha = B_z/B_{yz}, \cos\alpha = B_y/B_{yz}$, and $B_{yz} = (B_y^2 + B_z^2)^{1/2}$ [*Fitzenreiter et al.*, 1990]. The x component therefore remains unchanged, **B** lies entirely in the $x - y'$ plane, and the shock is still characterized by the same parameters a_s and b_s. For electrons to reach the observer from the tangent point, the spacecraft's z' coordinate necessarily equals the z' coordinate of the tangent point. Accordingly,

$$\begin{aligned} x'_T &= a_s - b_s\,(y'^2_T + z'^2_T) \\ z'_T &= z'_{sc} \\ x'_{sc} &= x_{sc};\ x'_T = x_T \end{aligned} \tag{8}$$

Standard foreshock theory yields one more relation [e.g., *Filbert and Kellogg*, 1979; *Cairns*, 1987a; *Fitzenreiter et al.*, 1990]:

$$y'_T = \frac{\cos\theta_{bu}}{2b_s\,\sin\theta_{bu}}, \tag{9}$$

where θ_{bu} is the angle between the solar wind bulk velocity and the IMF vector. Thus if b_s is considered known, a_s can be calculated in terms of the time lag, the solar wind speed, the spacecraft position, and the IMF orientation:

$$a_s = x_{sc} - V_{sw}\,(T_{\rm Langmuir} - T_{\rm Diff}) + b_s\,(y'^2_T + z'^2_T). \tag{10}$$

Here the implicitly written y'_T and z'_T can be obtained from (7), (8), and (9) .

In applying this formula, $b_s(P_{sw})$ is given by (2), with $P_0 = 1.69 \times 10^{-2}$ nPa, and P_{sw} is the ram pressure averaged over the interval from $T_{\rm Diff}$ to $T_{\rm Langmuir}$. There are some sources of uncertainty in deriving a_s, in par-

ticular in identifying the time T_{Diff}. Therefore the a_s value for a given event consists of a best estimate calculated from the best estimate for T_{Diff} and an error bar that depends on the maximum and minimum values for T_{Diff}.

Consider Figure 5 to see how the appearances and disappearances of Langmuir waves are correlated with changes in DIFF. After 0300 SCET on day 24 the spacecraft was within $\sim 35\,R_U$ of Uranus, so that electron beams with speeds of $\sim 10^7\,\mathrm{m\,s^{-1}}$ would take ~ 1 min to travel from the tangent point to the spacecraft. When computing the time lag, this electron propagation time should also be taken into account. At about 0305, DIFF jumped qualitatively from zero to positive values while the first wave event started at ~0317. It is persuasive that this change in DIFF is correlated with the wave onset at ~0317, resulting in a time lag of ~11 min after subtracting the ~1 min travel time for electrons. The IMF orientation is calculated by averaging the field vectors from 0305 to 0316, with a similar procedure for the spacecraft position. Equation (10) then yields the best estimate $a_s = 24.0\,R_U$. On the other hand, the time for the qualitative change in DIFF lies between 0301 and 0307 (Figures 5b and 5c). These two limits for T_{Diff} yield an error bar whose ends are $a_s = 21.2$ and $25.1\,R_U$, respectively.

Another example involves the abrupt change in DIFF from positive to negative values near 0453, with a best estimate $T_{\mathrm{Diff}} = 0453$. After a delay of ~6 min, Langmuir waves reappeared again, following about a 10-min absence of wave events. This delay can be interpreted in terms of the spacecraft initially being inside the ion foreshock (instead of the solar wind) before the favorable magnetic field lines appeared. It is evident, however, that (10) is also satisfied in this case. Deducting 1 min for the electron travel time, one obtains $a_s = 25.6\,R_U$. In addition, since T_{Diff} lies in the range 0452 to 0454, a_s lies in the range 24.7 to $26.7\,R_U$.

These two examples demonstrate the feasibility and usefulness of the lag time method. More events in which changes in DIFF are linked with the appearance or disappearance of Langmuir waves are identified in Figure 5 using open circles. Once the favorable magnetic fields reach the shock, Langmuir waves will be seen continuously until the fields at the spacecraft become unfavorable. Thus during such periods the basic remote sensing method can be applied since the favorable magnetic fields stably reach the bow shock. Averaging the IMF over the time T_{Lag} with Langmuir wave activity, (4) can be used to calculate a_s. We call this method the lagged-basic method. To obtain a_s and its estimated error, the following precedure is adopted. First, we calculate a_s using (4) with the value $b_s(P_{sw})$ predicted by (2) and the average (lagged) field orientation and the average spacecraft location for the time period. Second, we split the interval into two equal lengths, average the lagged IMF and the spacecraft position over these half intervals, and subsequently calculate a_s using (4). Three periods analyzed using this combined technique are denoted by solid circles in Figure 5. The a_s values inferred for day 24 using the lag time and lagged-basic methods are shown in Figure 8 using open squares or solid squares, respectively, and discussed in section 6.

On day 23, Voyager 2 was rather far away from Uranus, i.e., $x \sim 70\,R_U$. Approximately 60 min is then required for the solar wind to convect from the spacecraft to the bow shock. (The shock should have been stably located during this period according to the plasma science (PLS) solar wind data; see section 6.) Unfortunately, the IMF showed large-scale fluctuations and was often nearly radial on this day. These factors make it hard to identify correlated DIFF and Langmuir wave events on day 23. However, one event shows a clear relation between DIFF and Langmuir wave activity. At ~0445, DIFF first changed qualitatively to positive values, while Langmuir waves first appeared at ~0550. Deducting ~3 min for the electron travel time, this ~62-min time lag gives a nose position of the bow shock at $\sim 24.2\,R_U$ (not shown), which is reasonable. In summary, the new lag time method has been used successfully to remotely infer the location and motion of Uranus' bow shock on day 24, with some success for day 23.

5. Trace-back Method

The lag time method is reasonably successful at estimating the bow shock's standoff distance as a function of time, particularly on day 24. However, some wave events are not clearly associated with changes in DIFF, for example, from 0427 to 0447 and at 0549 in Figure 5, thereby precluding estimates of a_s for those times. Since the DIFF calculation assumes a nominal shock model with $a_s = 23.4\,R_U$, intrinsic shock motions have no associated signature in DIFF. In this section we will introduce a new technique, the trace-back method, to infer the bow shock's location and motion. This technique is independent from and complementary to the lag time analysis. It is the only applicable technique when Voyager was very close to the bow shock crossing, i.e., after 0700 on day 24. Convection of the frozen-in magnetic field by the solar wind plays an important part in the trace-back analysis.

Electron Beam Paths

Again, the energetic electron beams are assumed to travel along magnetic field lines to a very good approximation since their speeds greatly exceed the $\mathbf{E} \times \mathbf{B}$ drift speed. This makes it possible to calculate the trajectories along which electron beams reach the spacecraft by tracing back the IMF convected with the solar wind. Once the possible electron beam path that ends at the observer's position has been drawn for a given time period (taking the electron travel time into account), we can judge whether it properly connects to the bow shock

or not, according to the presence or absence of Langmuir waves, and then estimate the bow shock's location. It is important to consider the effects of fluctuations and other time variations in **B** which can cause the electron path to differ considerably from that derived solely using the time-averaged IMF direction.

The electron beam path can be constructed as follows. Suppose $\mathbf{s}(x, y, z)$ locates an arbitrary point on the path. Because electrons move along magnetic field lines, the tangent to the path at any point should be aligned with the IMF, i.e.,

$$(dx, dy, dz) = d\mathbf{s} = ds\hat{B} \tag{11}$$

where $\hat{B}$ is the magnetic field's unit vector. Integrating from the starting point (x_0, y_0, z_0), the coordinates of any point along the path are

$$\begin{aligned} x &= x_0 + \int_{x(t_i)}^{x(t_f)} dx \\ y &= y_0 + \int_{x(t_i)}^{x(t_f)} dx \frac{B_y(x)}{B_x(x)} \\ z &= z_0 + \int_{x(t_i)}^{x(t_f)} dx \frac{B_z(x)}{B_x(x)} \end{aligned} \tag{12}$$

Here t_i refers to the starting time and t_f indicates the ending time ($t_f > t_i$).

Further progress requires that $\mathbf{B}(x, y, z)$ be specified using the time-varying, single-point, IMF data measured by Voyager 2. A planar slab model is used with a grid spacing $L/\cos\theta$, where $L = V_{sw}\Delta t$ and θ is the angle between the mean magnetic field and the solar wind bulk velocity. The magnetic field is then constant in each grid volume, corresponding to slabs with the frozen-in IMF field measured by Voyager every $\Delta t = 1.92$ s that convect with the solar wind. Retaining an arbitrary slab normal $\mathbf{n} = (\cos\alpha, \cos\beta, \cos\gamma)$ for now and converting the integral to an approximate sum, (12) becomes

$$\begin{aligned} x(t_n) &= x_0(t_0) - L\cos\alpha \sum_{k=1}^{n} \frac{B_x(t_k)}{\mathbf{B}(t_k).\mathbf{n}} \\ y(t_n) &= y_0(t_0) - L\cos\beta \sum_{k=1}^{n} \frac{B_y(t_k)}{\mathbf{B}(t_k).\mathbf{n}} \\ z(t_n) &= z_0(t_0) - L\cos\gamma \sum_{k=1}^{n} \frac{B_z(t_k)}{\mathbf{B}(t_k).\mathbf{n}} \end{aligned} \tag{13}$$

The points $[x(t_j), y(t_j), z(t_j)]$, with $t_j = t_0 - 1.92j$ measured in s and $j = 0, 1, 2, \ldots, n$, then construct the path that electrons move along to reach the spacecraft at the arrival time t_0 for various previous "starting" times t_n.

Figure 6 schematically shows this procedure. A plot for the time-varying magnetic field is also included (only the x component is shown). Suppose t_0 is the electron arrival time (or ending time) and t_n is the starting time. First, we draw a dashed-line grid imposed in the x axis (the solar wind flow direction) with spacing $L = V_{sw}\Delta t$; then along the solar wind direction we place thin solid line vectors sequentially into the dashed grid points in inverse order of time ($t_0 > t_1 \ldots, > t_n$). The grid de-

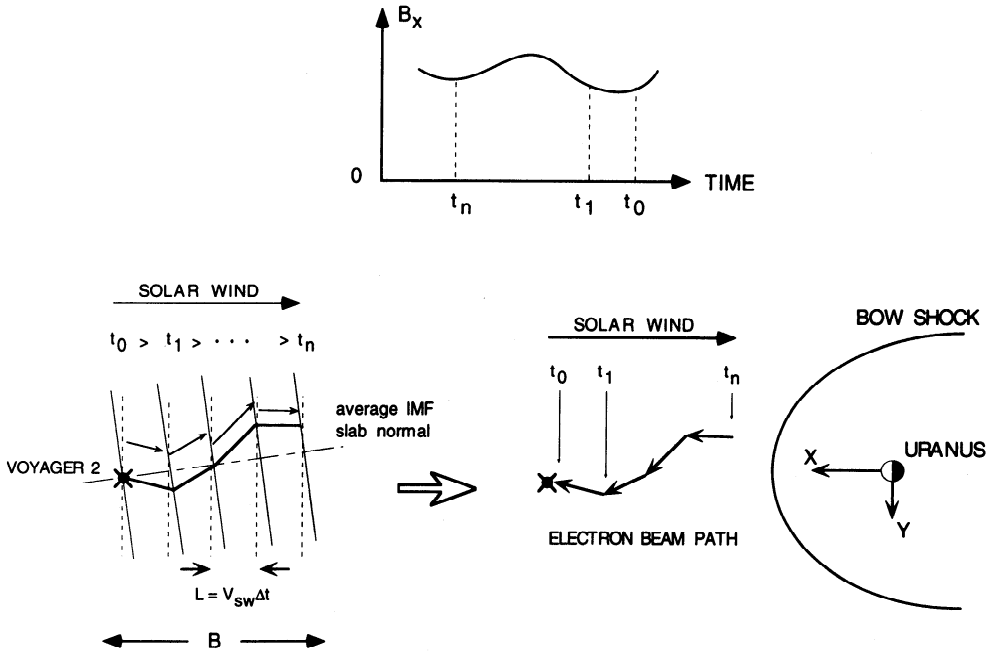

Figure 6. A schematic illustrating the construction of electron beam paths using the trace-back method. More detailed explanations are given in the text.

fined in the preceding paragraph is imposed in the average IMF direction (the solid lines perpendicular to the dashed slanted line, i.e., the average IMF). Then starting from the spacecraft, we draw straight lines across the grid by joining the thin solid line field vectors. The electron path is thus shown by the continuous thick solid line.

In the following, we primarily adopt the familar model of slabs oriented perpendicular to the mean magnetic field [*Belcher and Davis*, 1971]. This geometry is one-dimensional, with finite correlation length along the mean field and infinite correlation lengths perpendicular to the mean field, so that the IMF does not vary under translations across the mean field. *Matthaeus et al.* [1990, 1995, and references therein] demonstrate, however, that IMF fluctuations often have a significant two-dimensional component that provides a finite correlation length for translation across the mean field. These analyses used hour-averaged data for much larger spatial scales than analyzed here. Little is known about the geometry of fluctuations at spatial scales related to seconds and minutes of IMF data. Possible errors resulting from the slab assumption are partially mitigated by, first, the fact that the spacecraft-to-shock distance is much smaller than the nominal correlation lengths parallel or perpendicular to the mean IMF and, second, the use of relatively high resolution IMF data that minimize the step size L to be much smaller than the correlation lengths. Using only the single-point Voyager data, it is not possible to avoid errors associated with the significant three-dimensional spatial variations (scales $\gtrsim 5 \times 10^6$ m) often seen in the solar wind. At this stage, however, we proceed using the slab model with normals perpendicular to the average IMF while recognizing both the limitations and apparent necessity of this assumption. Different slab orientations, i.e., normal to the radial direction, can yield somewhat different results, as discussed in section 6. Below, the slab orientation used for a given event is given by the average IMF direction calculated between an event's starting and ending time. The constant solar wind speed used is the average value over the same time interval.

Estimating Limits on the Bow Shock Standoff Distance

When Langmuir waves are present, the electron path should properly connect the spacecraft to the bow shock. Conversely, without a proper connection to the shock there should be no Langmuir waves. There are then two basic ways to infer the standoff distance. Both methods assume the shape $b_s(P_{sw})$ given by (2). The choice between the two depends upon the actual structure of the electron paths.

Figure 7 shows the electron beam path between 0300 and 0317 on day 24 using projections onto the x-y and x-z planes. The nominal shock model with $a_s =$

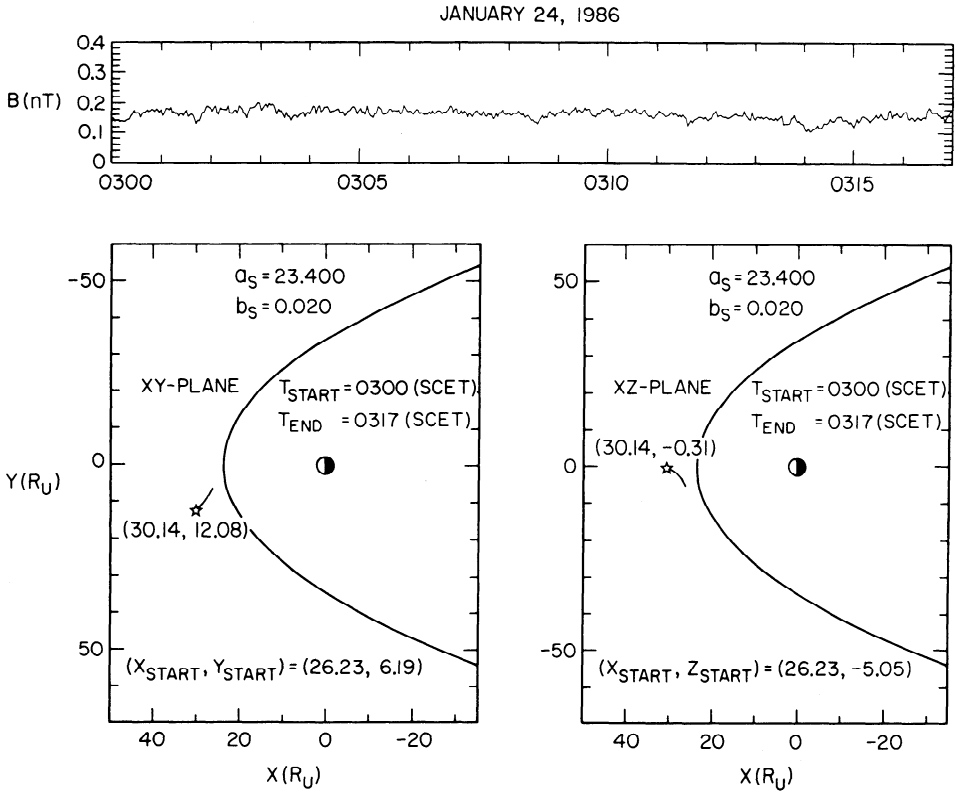

Figure 7. Electron beam path calculated for the period 0300-0317 SCET (180-197 min). The point (x_{start}, y_{start}) and the star refer to the starting point and the ending point of the path, respectively.

$23.4\,R_U$, $b_s = 0.02\,R_U^{-1}$ is plotted for comparison. The IMF magnitude during this period is shown in Figure 7 (top). (The reason for showing this is discussed in the next subsection.) At 0317, Langmuir waves occurred (see Figure 5). This means that the electron path (and the magnetic field line) connects the spacecraft to the bow shock. The first method for estimating a_s involves regarding the electron path as an imaginary tangent magnetic field line that reaches the shock. The "tangent" magnetic field line is computed by connecting the two ends of the electron path with a straight line. Then the basic remote sensing equation (4) enables us to calculate a_s when b_s is assumed known, thereby giving us the shock's location. Suppose the bow shock was located closer to the planet than the end of the electron path; then the spacecraft would be upstream from the electron foreshock and no Langmuir waves could be observed. This would be a contradiction. Therefore the inferred a_s actually is a lower limit to the standoff distance. Using (4), the lower limit on a_s at 0317 is $23.3\,R_U$. A similar procedure yields an upper limit on a_s when no Langmuir waves are present.

When the spacecraft was very close to the bow shock, i.e., from 0700 on day 24 until the inbound shock crossing at 0728, the first method is no longer viable. This is because Langmuir waves were absent during this period or were too weak when they did occur (see Figure 5). It is then difficult to identify the proper tangent magnetic field line since the spacecraft was very probably deep in the electron foreshock or in the ion foreshock. However, the spacecraft must be located upstream from the shock before 0728 SCET in the absence of evidence for additional shock crossings. Then supposing that (x_{sc}, y_{sc}, z_{sc}) lies on the bow shock surface given by (1),

$$a_s' = x_{sc} + b_s(y_{sc}^2 + z_{sc}^2) \qquad (14)$$

is obviously an upper limit for a_s. Recapping, the above approaches for using the trace-back method to place limits on a_s are all based on the following relationships: Langmuir waves appear $\Rightarrow$ lower limits on a_s and Langmuir waves disappear $\Rightarrow$ upper limits on a_s .

The limits on a_s calculated for day 24 using these methods are shown in Figure 8 using arrows. The times selected for this analysis are indicated in Figure 5 by stars. Comparing in Figure 8 the lag time (open circles), the lagged-basic (solid circles), and the trace-back results (arrows), it is clear that these analyses all yield a reasonably clear and consistent picture for the standoff distance on day 24. In the next section these estimates are compared with those predicted using MHD theory and the observed plasma parameters.

Discussion

The trace-back method appears useful in assessing the location of Uranus' bow shock and is a good complement to the lag time method. Nevertheless, several aspects of the analysis need further discussion.

The first problem that might be noted is whether Maxwell's equation $\nabla \cdot \mathbf{B} = 0$ is satisfied when constructing the electron beam paths. In fact, this requirement is not strictly satisfied. Visualized in terms of magnetic field lines, the divergence equation implies that magnetic field lines are continuous throughout space. Variations in field strength correspond to the number density of field lines. A basic assumption is made in our construction, i.e., that the IMF is uniform in the y-z plane at each x grid position. Further, it is supposed that the magnetic field lines in neighboring regions connect with each other. Strictly speaking this violates $\nabla \cdot \mathbf{B} = 0$ because changes in the actual IMF magnitude correspond to different densities of field lines, thereby resulting in discontinuities at the boundaries of neighboring regions. However, when the fluctuations in the measured IMF are relatively small compared to the average field strength, e.g., <10–20%, the above assumption should still be approximately satisfied. Thus care must be taken in selecting the intervals for which to construct electron paths. If the IMF strength varies significantly during a certain period, then the calculated electron path should be rejected. This is why we included plots of B as a function of time in Figure 7. Unfortunately, this situation cannot be improved without more information on the spatial variability of the IMF. For instance, we need magnetic field data from two spacecraft operating simultanously.

Lastly, both the trace-back and the lag time methods assume that slab models are viable. As discussed earlier, no other option is presently available. Summarizing, some potential problems cannot always be effectively avoided. These difficulties have been minimized by carefully choosing intervals for analysis.

6. Comparison With Theory

Variations in the upstream solar wind ram pressure, the sonic (M_S), Alfvén (M_A), and fast magnetosonic (M_{MS}) Mach numbers, the IMF orientation, and the magnetopause location and shape affect the location and shape of planetary bow shocks [e.g., *Spreiter et al.*, 1966; *Binsack and Vasyliunas*, 1968; *Fairfield*, 1971; *Formisano et al.*, 1971; *Slavin and Holzer*, 1981; *Slavin et al.*, 1985; *Farris et al.*, 1991; *Russell and Zhang*, 1992; *Cairns and Grabbe*, 1994; *Cairns et al.*, 1995; *Cairns and Lyon*, 1995]. Recent work has shown that models based on gasdynamics, with or without phenomenological substitution of M_A or M_{MS} for M_S, are observationally [*Russell and Zhang*, 1992; *Cairns et al.*, 1995] and theoretically inadequate at low Alfvén (or fast mode) Mach numbers due to intrinsically MHD effects becoming important [*Cairns and Grabbe*, 1994; *Cairns and Lyon*, 1995]. Furthermore, even at high Mach numbers, MHD effects lead to different asymptotic magnetosheath thicknesses than for models based on gasdynamics.

Balancing the solar wind ram pressure with the magnetostatic pressure of the planetary magnetic dipole

(higher-order components should be ignorable at the magnetopause), it is expected that $a_s \propto P_{sw}^{-1/6}$, as observed for Earth. As mentioned previously, a_s is generally also a function of the Mach numbers, the magnetic field orientation, and the magnetopause shape. For instance, MHD simulations of flows with $M_A \sim 1.5-10$, $M_S = 7.6$, and the solar wind magnetic field oriented at $\theta = 45°$ and 90° relative to the solar wind velocity yield [*Cairns and Lyon*, 1995]

$$a_s = CP_{sw}^{-1/6}(1 + 3.4X - 0.6). \quad (15)$$

Here $X = \rho_{sw}/\rho_d$ is the density jump at the shock given by a cubic equation derived from the MHD Rankine-Hugoniot conditions [e.g., *Cairns and Grabbe*, 1994] that involves M_A, M_S, θ, and the adiabatic index γ. A popular modified-gasdynamics model for a_s is [e.g., *Formisano et al.*, 1971; *Farris et al.*, 1991]

$$a_s = CP_{sw}^{-\frac{1}{6}}\left(1 + 1.1\frac{(\gamma-1)M_{MS}^2 + 2}{(\gamma+1)M_{MS}^2}\right) \quad (16)$$

where M_{MS} has been substituted for M_S in the gasdynamics result of *Spreiter et al.* [1966]. In these cases the constants 3.4, 0.6, and 1.1 are peculiar to Earth's magnetopause; for instance, models for Venus use (16) with 0.8 instead of 1.1. Equations (15) and (16) also give slightly different absolute values for a_s at large Mach numbers. Fortunately, these uncertainties in magnetopause shape and the Mach number models can be removed here.

The solar wind plasma parameters for Voyager's encounter with Uranus were measured by the Voyager 2 PLS instrument [*Bridge et al.*, 1977] and provided by A. Szabo and J. W. Belcher (personal communication, 1992). The PLS data shown below and by *Bagenal et al.* [1987] demonstrate that Voyager's inbound pass took place during a period of high $M_A \gtrsim 10$, high $M_S \gtrsim 30$, and high $M_{MS} \gtrsim 10$, so that Mach number effects on the shock's location are essentially ignorable. In particular, in this high Mach number regime the gasdynamics model [*Spreiter et al.*, 1966], the modified-gasdynamics models formed by substituting M_{MS} or M_A for M_S in the gasdynamics model [*Fairfield*, 1971; *Formisano et al.*, 1971; *Farris et al.*, 1991], and the MHD models [*Cairns and Grabbe*, 1994; *Cairns and Lyon*, 1995] all yield predictions for a_s that differ by $\lesssim 1\%$. Uncertainties regarding the magnetopause shape and the magnetosheath thickness can be removed in this regime, provided inaccuracies of $\lesssim 1\%$ are acceptable, by taking

$$a_s = CP_{sw}^{-1/6}, \quad (17)$$

ignoring the Mach number dependence, and normalizing relative to the value $a_s = 23.4R_U$ and the solar wind conditions for the inbound shock crossing (thereby determining C). In this case, only variations in P_{sw} cause the shock to move. Applying the normalized version of (17) to the M mode PLS data (12-min time resolution), the predicted time variations of a_s on day 24 are plotted in Figure 8 using asterisks. Hereafter, these a_s values are said to be provided by the "standard model".

We find that the model gives standoff distances that were relatively stable on both days, especially on day 24. Before ~1500 on day 23, a_s is predicted to be relatively constant at $\sim 26 \pm 1\, R_U$; in the remainder of the day, the predicted a_s lie in the range $24-28\, R_U$. While Langmuir waves were observed on day 24, from ~0320 to ~0650, the predicted a_s values are very stably near $\sim 23.4\, R_U$. The solar wind data therefore provide no indication that Uranus' bow shock should have moved back and forth very quickly, as predicted by the basic remote sensing analysis (section 3) during the period 0310–0340 on day 24. It is this inconsistency that led us to establish the two independent modified remote sensing techniques.

Figure 8 compares the standoff distances for Uranus' bow shock calculated using the modified remote sensing analyses with the shock positions predicted using the standard model. The open circles and the solid circles show the lagtime and the combined lagged-basic results, and the solid arrows represent the trace-back limits.

Figure 8 shows that, first, the results from the lag time and trace-back methods are consistent for the periods when both techniques are available. Second, from ~0315 to 0320, the remotely sensed shock locations were qualitatively consistent with the predictions from the standard model. For instance, these analyses indicate that $a_s \sim 23 \pm 2\, R_U$, as predicted by the standard model. Third, when the spacecraft moved very close to the bow shock (after 0700), the remotely sensed standoff distance clearly tended toward the value $23.4\, R_U$ inferred from the inbound shock crossing. These results demonstrate that our modified remote sensing analyses are working effectively. However, Figure 8 shows that differences also apparently exist between the remotely sensed and model shock locations for the period of ~0340 to 0700 as follows: the remotely sensed a_s values have a maximum value of $\sim 29\, R_U$ near ~0350, while the model prediction remains near $\sim 23\, R_U$. Note that the Langmuir waves observed when DIFF ~-10–0 R_U during the period 0340–0700 for the nominal shock model (Figure 5) imply that, actually, $a_s \sim 23-33\, R_U$ during this period, thereby agreeing with the remote sensing results. The discrepancy cannot be interpreted in terms of the standard model (17) and the observed solar wind ram pressure and Mach numbers.

It is possible that these differences in the predicted and remotely sensed standoff distance for the period 0350–0700 are an artifact of the analyses. Careful review of the remote sensing techniques has not identified any systematic errors in the independent trace-back and lag time methods. Therefore the discussion below assumes that the differences in Figure 8 are real.

Ness et al. [1986] suggested that the rotation of Uranus' oblique, tilted dipole should lead to intrinsic changes in bow shock location and/or shape in addition to those caused by variations in the ram pres-

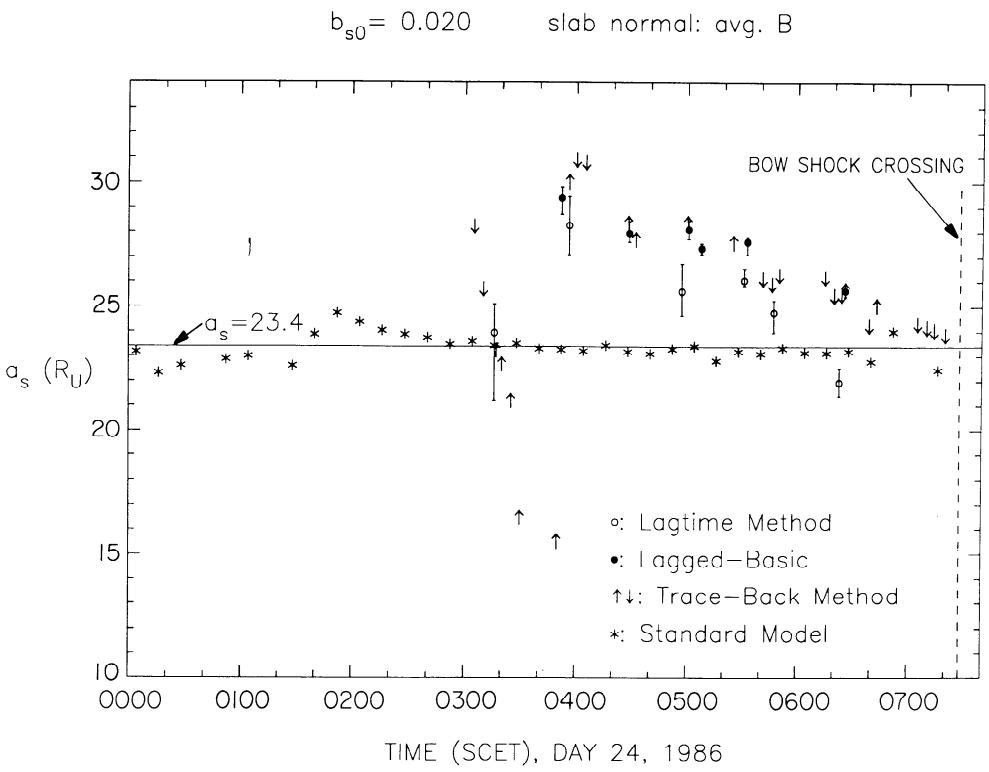

Figure 8. A comparison of the remote sensing results and the predictions of the standard model. The open circles and the solid circles show the lag time and the combined lagged-basic results, and the solid arrows represent the trace-back limits with upward pointing arrows and downward pointing arrows indicating lower limits and upper limits on a_s, respectively. The a_s predicted values by the standard model are shown by asterisks.

sure and/or Mach number, in particular, an asymmetric bulge that rotates at Uranus' rotation rate. Similar suggestions have been made for Neptune [*Ness et al.*, 1989; *Belcher et al.*, 1989], and experimental evidence for these variations exists [*Cairns et al.*, 1991; *Szabo*, 1992]. Uranus has an approximately 17-hour rotation period, while effective remote sensing was possible only during an approximately 4-hour period on day 24 (~0320–0730). This duration is therefore too short to see periodic changes in the shock's standoff distance. Nevertheless, we attempted to see whether our data are consistent with *Ness et al.*'s [1986] suggested rotating bulge. If the bulge exists and the spacecraft is magnetically connected to the bulge when Langmuir waves are observed, then the inferred a_s should be larger than the actual nose position. This effect could therefore potentially explain the differences between the remote sensing results and the model predictions. At present, however, analyses of the magnetic latitude and longitude of the connection site on the shock (inferred using the remotely sensed shock location and the IMF data) do not show any strong evidence for or against this model.

Another possible explanation is that the shock's symmetry axis is not the Sun-Uranus line (i.e., due to a bulge) and that Uranus's rotation causes the symmetry axis of the shock to rotate about the Sun-Uranus line, thereby making the shock appear asymmetric at any given time. Qualitatively, it is plausible that the present remote sensing analyses, which assume symmetry about the Sun-Uranus line, would interpret this asymmetry in terms of increased or decreased a_s values from those predicted by (15). Further work is necessary to test this explanation and the above "bulge" model.

Before concluding, we address the effect of different slab orientations on the trace-back results and a plausible way of identifying b_{s0}. Figure 9 is an analogue of Figure 8 except that $b_{s0} = 0.014\,R_U^{-1}$ and the trace-back results are calculated assuming the shock normals are aligned with the x axis (i.e., radial symmetry). Figure 10 is identical to Figure 9 except that the slabs normals are aligned with the average IMF direction. There is a larger difference between the trace-back results and the lag time and lagged-basic results in Figure 9 than in Figure 10. This suggests that the slabs are most plausibly perpendicular to the average IMF direction. Comparing Figures 8 and 10, which differ only in the choice of b_{s0}, shows better agreement between the trace-back and other remote sensing results. Ideally, if both techniques are correct and do not suffer from systematic errors, the two techniques should give essentially identical results. It is plausible (but not certain) that for the true value of b_{s0} the differences between the two techniques would be minimized. We therefore calculated and compared analogues of Figures 8 and 10 for b_{s0} =0.010–0.024 R_U^{-1},

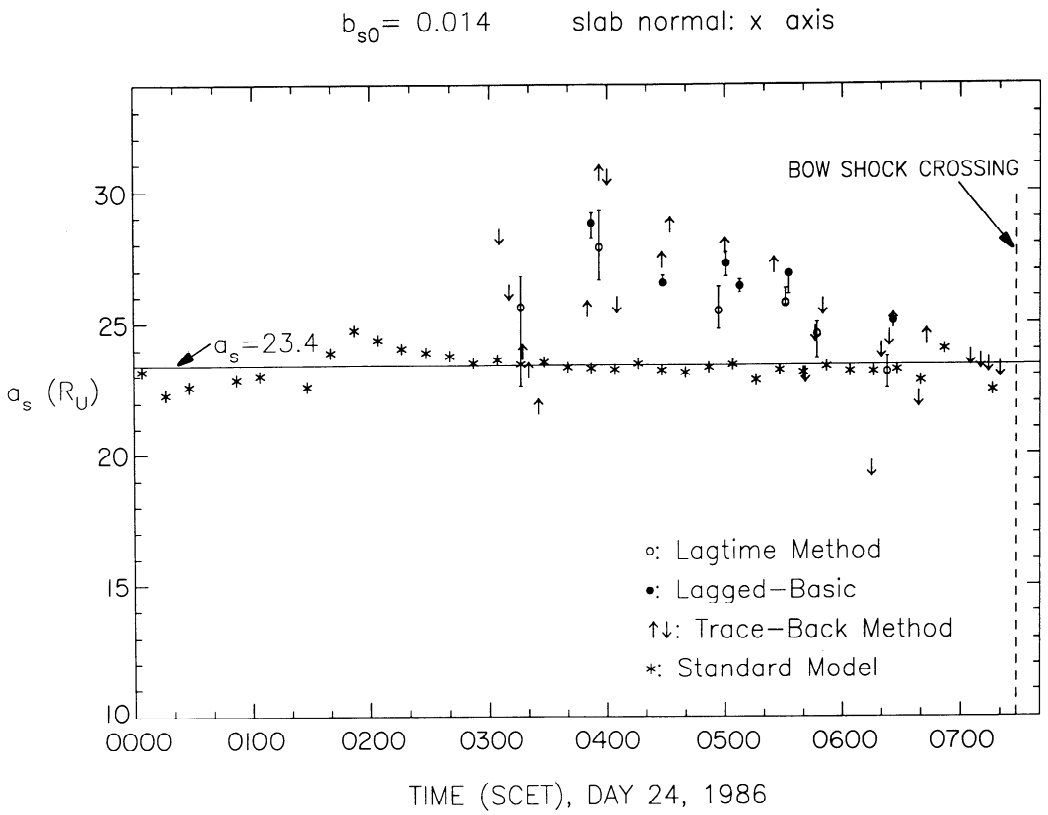

Figure 9. An analogue of Figure 8, except that $b_{s0} = 0.014\,R_U^{-1}$ and the trace-back results are calculated assuming that the slab normals are aligned with the x axis.

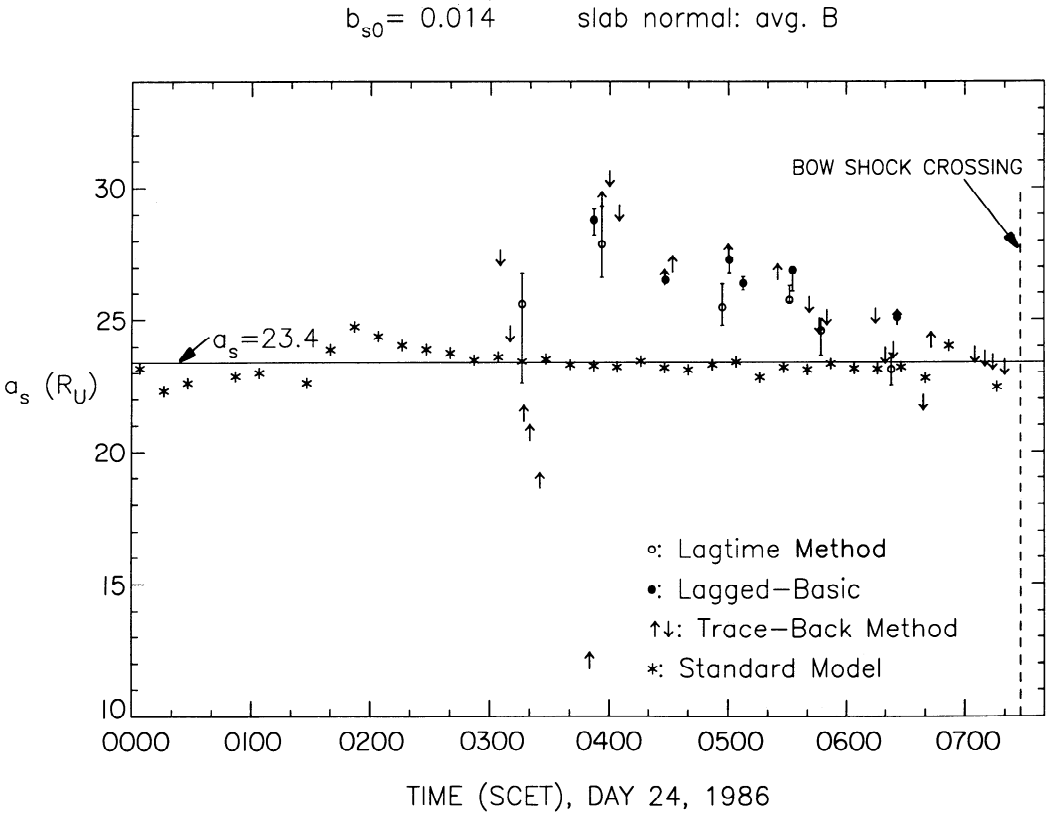

Figure 10. Similar to Figure 9 with $b_{s0} = 0.014\,R_U^{-1}$, except that the slabs normals are aligned with the average IMF orientation.

in steps of $0.001\,R_U^{-1}$. The results suggest that the best estimate of b_{s0} should be $0.014\,R_U^{-1}$, somewhat smaller than the nominal value calculated from the inbound and first outbound shock crossings.

7. CONCLUSIONS

Remote sensing analyses have been performed to estimate semiquantitatively the location and motion of Uranus' bow shock prior to the inbound bow shock crossing using Langmuir wave and magnetic field data. These analyses include two new independent techniques, the lag time method and the magnetic field trace-back method, in addition to a previous technique (the basic remote sensing analysis). The bow shock is assumed to have a paraboloidal shape symmetric about the Sun-Uranus line, with the flaring parameter b_s varying self-consistently with P_{sw}. We used the magnetic fields and spacecraft positions associated with Langmuir wave events to infer the standoff distance of the bow shock. Our results may be summarized as follows. First, we have shown that the observed Langmuir waves are qualitatively consistent with the standard electron foreshock model by inspecting the value of the parameter DIFF. Second, because the interplanetary magnetic field fluctuated much more than expected, the basic remote sensing analysis met some difficulties in properly determining the shock standoff distance. It was therefore necessary to modify the analysis technique. Third, the modified analyses, the lag time method and the complementary trace-back method, found that the standoff distance of Uranus' bow shock was relatively stable around $\sim 25\,R_U$ for much of the period when Langmuir waves were detected on January 24, 1986. This is consistent with the shock positions predicted on the basis of the observed plasma parameters and the standard shock model. Fourth, the remote sensing results imply that the standoff distance is sometimes significantly greater than predicted from variations in the solar wind ram pressure and Mach number. A definitive explanation for this difference is not yet known. It may be due to limitations in the remote sensing analyses associated with nonperpendicular magnetic slab orientations (or other global IMF structures) or to modulation of the shock's location and/or shape at Uranus' rotation period. Lastly, these analyses illustrate the difficulties in precisely describing the motion of a planetary bow shock using remote sensing techniques when the IMF is highly irregular.

Despite the difficulties mentioned above, the remote sensing analyses have enjoyed considerable success. No other method is presently known for remotely sensing bow shock positions. Ideally, an orbiter would provide a more complete data set for further studying bow shock motions and for investigating wobble effects related to the planetary rotation. In the future we hope to study other planetary bow shocks using these remote sensing techniques.

Acknowledgments. This work was supported by the NASA grant NAGW-2040, NSF grant ATM-9021985 and the JPL Contract 959193 to the University of Iowa and by the NASA grant NAGW-3445 and the JPL Contract 959167 to the Bartol Research Institute.

The Editor thanks P. J. Kellogg and M. D. Desch for their assistance in evaluating this paper.

References

Anderson, R. R., G. K. Parks, T. E. Eastman, D. A. Gurnett, and L. A. Frank, Plasma waves associated with energetic particles streaming into the solar wind from the Earth's bow shock, *J. Geophys. Res., 86*, 4493, 1981.

Bagenal, F., J. W. Belcher, E. C. Sittler Jr., and R. P. Lepping, The Uranian bow shock: Voyager 2 inbound observations of a high Mach number shock, *J. Geophys. Res., 92*, 8603, 1987.

Behannon, K. W., M. H. Acuna, L. F. Burlaga, R. P. Lepping, N. F. Ness, and F. M. Neubauer, Magnetic field experiment for Voyagers 1 and 2, *Space Sci. Rev., 21*, 235, 1977.

Belcher, J.W., and L. Davis Jr., Large amplitude Alfvén waves in the interplanetary medium. 2, *J. Geophys. Res., 76*, 3534, 1971.

Belcher, J. W., et al., Plasma observations near Neptune: Initial results from Voyager 2, *Science, 246*, 1478, 1989.

Binsack, J.H., and V.M. Vasyliunas, Simultaneous IMP 2 and OGO 1 observations of bow shock compression, *J. Geophys. Res., 73*, 429, 1968.

Bonifazi, C., and G. Moreno, Reflected and diffuse ions backstreaming from the Earth's bow shock, 2, Origin, *J. Geophys. Res., 86*, 4405, 1981.

Bridge, H. S., J. W. Belcher, R. J. Butler, A. J. Lazarus, A. M. Mauretic, J. D. Sullivan, G. L. Siscoe, and V. M. Vasyliunas, The plasma experiment on the 1977 Voyager mission, *Space Sci. Rev., 21*, 259, 1977.

Bridge, H. S., et al., Plasma observations near Uranus: Initial results from Voyager 2, *Science, 233*, 89, 1986.

Cairns, I. H., The electron distribution function upstream from the Earth's bow shock, *J. Geophys. Res., 92*, 2315, 1987a.

Cairns, I. H., A theory for the Langmuir waves observed upstream from the Earth's bow shock, *J. Geophys. Res., 92*, 2329, 1987b.

Cairns, I. H., and C. L. Grabbe, Towards an MHD theory for the standoff distance of Earth's bow shock, *Geophys. Res. Lett., 21*, 2781, 1994.

Cairns, I. H., and J. G. Lyon, MHD simulations of Earth's bow shock at low Mach numbers: Standoff distances, *J. Geophys. Res., 100*, 17,173, 1995

Cairns, I. H., C. W. Smith, W. S. Kurth, D. A. Gurnett, and S. Moses, Remote sensing of Neptune's bow shock: Evidence for large-scale shock motions, *J. Geophys. Res., 96*, 19,153, 1991.

Cairns, I. H., D. H. Fairfield, R. R. Anderson, V. E. H. Carlton, K. I. Paularena, and A. J. Lazarus, Unusual locations of Earth's bow shock on September 24 - 25, 1987: Mach number effects, *J. Geophys. Res., 100*, 47, 1995.

Etcheto, J., and M. Faucheux, Detailed study of electron plasma waves upstream of the Earth's bow shock, *J. Geophys. Res., 89*, 6631, 1984.

Fairfield, D.H., Average and unusual locations of the Earth's magnetopause and bow shock, *J. Geophys. Res., 76*, 6700, 1971.

Farris, M. H., S. M. Petrinic, and C. T. Russell, The thickness of the magnetosheath: Constraints on the polytropic index, *Geophys. Res. Lett., 18*, 1821, 1991.

Filbert, P. C., and P. J. Kellogg, Electrostatic noise at the plasma frequency beyond the Earth's bow shock, *J. Geophys. Res., 84*, 1369, 1979.

Fitzenreiter, R. J., J. D. Scudder, and A. J. Klimas, Three-dimensional analytical model for the spatial variation of the foreshock electron distribution function: Systematics and comparisons with ISEE observations, *J. Geophys. Res., 95*, 4155, 1990.

Formisano, V., P. C. Hedgeock, G. Moreno, J. Sear, and D. Bollea, Observations of Earth's bow shock for low Mach numbers, *Planet. Space Sci., 19*, 1519, 1971.

Fuselier, S. A., D. A. Gurnett, and R. J. Fitzenreiter, The downshift of electron plasma oscillations in the electron foreshock region, *J. Geophys. Res., 90*, 3935, 1985.

Fuselier, S. A., W. C. Feldman, S. J. Bame, E. J. Smith, and F. L. Scarf, Heat flux observations and the location of the transition region boundary of Giacobini-Zinner, *Geophys. Res. Lett., 13*, 247, 1986.

Gary, S. P., C. W. Smith, M. A. Lee, M. L. Goldstein, and D. W. Forslund, Electromagnetic ion beam instabilities, *Phys. Fluids, 27*, 1852, 1984.

Gurnett, D. A., W. S. Kurth, and F. L. Scarf, Plasma waves near Saturn: Initial results from Voyager 1, *Science, 212*, 235, 1981.

Gurnett, D. A., W. S. Kurth, F. L. Scarf, and R. L. Poynter, First plasma wave observations near Uranus, *Science, 233*, 106, 1986.

Gurnett, D. A., et al., First plasma wave observations at Neptune, *Science, 246*, 1494, 1989.

Klimas, A. J., The electron foreshock, in *Collisionless Shocks in the Heliosphere: Reviews of Current Research, Geophys. Monogr. Ser.*, vol. 35, edited by B. T. Tsurutani and R. G. Stone, p. 237, AGU, Washington, D. C., 1985.

Krimigis, S. M., E. P. Keath, B. H. Mauk, A. F. Cheng, L. J. Lanzerotti, R. P. Lepping, and N. F. Ness, Observations of energetic ion enhancements and fast neutrals upstream and downstream of Uranus' bow shock by the Voyager 2 spacecraft, *Planet. Space Sci., 36*, 311, 1988.

Lepping, R. P., T. A. Vollmer, J. A. Jones, and N. F. Ness, Plots of Voyager 2 Uranus magnetic field data, report NASA Goddard Space Flight Cent., Greenbelt, MD., 1989.

Matthaeus, W. H., M. L. Goldstein, and D. A. Roberts, Evidence for the presence of quasi-two-dimensional nearly incompressible fluctuations in the solar wind, *J. Geophys. Res., 95*, 20,673, 1990.

Matthaeus, W. H., J. W. Bieber, and G. P. Zank, Unquiet on any front: Anisotropic turbulence in the solar wind, *U.S. Natl. Rep. Int. Union Geod. Geophys. 1991-1994, Rev. Geophys, 33*, 609, 1995.

Ness, N. F., M. H. Acuna, K. W. Behannon, L. F. Burlaga, J. E. P. Connerney, R. P. Lepping, and F. M. Neubauer, Magnetic field at Uranus, *Science, 233*, 85, 1986.

Ness, N. F., M. H. Acuna, L. F. Burlaga, J. E. P. Connerney, R. P. Lepping, and F. M. Neubauer, Magnetic fields at Neptune, *Science, 246*, 1473, 1989.

Robinson, P. A., I. H. Cairns, and D. A. Gurnett, Clumpy Langmuir waves in type III radio sources: Comparison of stochastic-growth theory with observations, *Astrophys. J., 407*, 790, 1993.

Russell, C. T., and T. L. Zhang, Unusually distant bow shock encounters at Venus, *Geophys. Res. Lett., 19*, 833, 1992.

Russell, C. T., R. P. Lepping, and C. W. Smith, Upstream waves at Uranus, *J. Geophys. Res., 95*, 2273, 1990.

Scarf, F. L., R. W. Fredericks, L. A. Frank, and M. Neugebauer, Nonthermal electrons and high-frequency waves in the upstream solar wind, 1, observations, *J. Geophys. Res., 76*, 5126, 1971.

Scarf, F. L., and D. A. Gurnett, A plasma wave investigation for the Voyager mission, *Space Sci. Rev., 21*, 289, 1977.

Scarf, F. L., D. A. Gurnett, and W. S. Kurth, Jupiter plasma wave observations: An initial Voyager 1 overview, *Science, 204*, 991, 1979.

Slavin, J. A., and R. E. Holzer, Solar wind flow about the terrestrial planets, 1, Modeling bow shock position and shape, *J. Geophys. Res., 86*, 11,401, 1981.

Slavin, J. A., E. J. Smith, J. R. Spreiter, and S. S. Stahara, Solar wind flow about the outer planets: Gas dynamic modelling of the Jupiter and Saturnian bow shocks, *J. Geophys. Res., 90*, 6275, 1985.

Smith, C. W., M. L. Goldstein, and H. K. Wong, Whistler wave bursts upstream of the Uranian bow shock, *J. Geophys. Res., 94*, 17,035, 1989.

Spreiter, J. R., A. L. Summers, and A.Y. Alksne, Hydromagnetic flow around the magnetospheres, *Planet. Space Sci., 14*, 233, 1966.

Szabo, A., The outbound Neptunian bow shock crossings of Voyager 2, paper presented at *Magnetospheres of the Outer Planets* Symposium, Los Angeles, Califo, June 22 - 26, 1992.

Voigt, G.-H., and N. F. Ness, The magnetosphere of Neptune: Its response to daily rotation, *Geophys. Res. Lett., 17*, 1705, 1990.

Zhang, M., J. W. Belcher, J. D. Richardson, Alfvén waves and associated energetic ions downstream from Uranus, *J. Geophys. Res., 96*, 1647, 1991.

I. H. Cairns and D. A. Gurnett, Department of Physics and Astronomy, University of Iowa, Iowa City, IA 52242. (email: ihc@space.physics.uiowa.edu and gurnett@iowave.physics.uiowa.edu)

C. W. Smith, Bartol Research Institute, University of Delaware, Newark, DE 19711. (email: chuck@bartol.udel.edu

S. Xue, Department of Space Physics and Astronomy, Rice University, P.O. Box 1892, Houston, TX 77251. (email: xue@space.rice.edu)

(Received September 19, 1995; revised December 15, 1995; accepted December 15, 1995.)